Chapter 3

3. BCN Assisted Electro-functionalization of SPE for Tryptophan Sensing

3.1 Introduction

Electrochemical sensors have firmly invaded the chemical sensing domain over the past decades owing to their on-site applicability, low cost, facile fabrication, high sensitivity, and selectivity[137–141]. Nevertheless, their performance and applicability are widely dependent on the scaffold that provides the interface for electrochemical processes, precisely on the working electrode in the three-electrode system. Compared to the conventional three-electrode system, the invention of screen-printed electrodes (SPE) has revolutionized the commercial deployment of electrochemical sensors for the qualitative and quantitative analysis of numerous food toxicants, environmental pollutants, industrial toxicants, and essential biological molecules[142–144]. It offers several benefits, like low sample volume requirement, tender pre-treatment or cleaning protocols, and portability for PoC devices. Interestingly, the sensitivity and stability of SPEs can be amplified by tailoring the electrode/analyte interface using materials that offer better conductivity, superior charge transfer, greater surface area, high stability, and desired specificity via surface functionalization. Researchers have shown great interest in exploring the potential of two-dimensional nanomaterials to bring breakthroughs in this field[145,146]. Owing to its unique morphological, electronic, and optical properties, 2D nanomaterials offer great promise for various applications. For this reason, graphene, reduced graphene oxide, boron nitride, transition-metal dichalcogenides (such as MoS_2, WS_2), and metal oxides have been widely investigated for improving the sensitivity and selectivity of the electrode surfaces[147–150]. Boron carbon nitride (BCN) has garnered recognition as a highly versatile

and multifunctional two-dimensional nanomaterial. Their electronic and optical properties can be fine-tuned to achieve unique distinctions from their parent materials, namely graphene and hBN. The properties of BCN materials can be effectively modulated to tailor for electrochemical applications. The BCN is expected to significantly enhance the electrochemical activity by decreasing the over-potential and increasing the current response for two reasons: an increase in surface area and the presence of nitrogen-rich groups on the modified surface. Furthermore, BCN is expected to exhibit strong π-π interactions with aromatic compounds, which provides an advantage in detecting molecules containing aromatic rings[151]. A thorough literature survey revealed only a few reports showcasing the utilization of BCN materials in modifying electrochemical sensing platforms. Sriram et al[152] successfully sensed furazolidone using a screen-printed carbon electrode modified with cobalt molybdate nanorods decorated BCN sheets. Zhu and group[153] decorated BCN nanosheets with hematite nanocrystals which were used to detect toxic lead ions in natural water electrochemically. The same Fe_2O_3-BCN composite was used in another research to modify GCE and employed the platform for determining paraquat in natural water[154]. In a study conducted by Peng et al[155], copper-decorated BCN nanosheets were deposited on GCE for electrochemical detection of the antibacterial antibiotic chloramphenicol. However, all the reported studies have employed simple drop-cast and heat-drying methods for electrode modifications. While a commonly used technique for surface modification of the working electrode, the drop-casting process has several drawbacks, such as unevenness of the modified layer and material leaching, which might instigate sensors to furnish inconsistent and unreliable results.

Here, we propose an approach for fabricating a highly selective and sensitive sensor by functionalizing commercial SPEs, which are low-cost, user-friendly, portable, and require only a small quantity of samples, making it ideal for point-of-care testing. The proposed

protocol for the functionalization of less-sensitive disposable electrodes holds promise for transforming the field of analytical chemistry, as the fabricated surface can provide swift and precise detection of a diverse range of analytes in real-world settings at an affordable cost. To investigate the practicality of the proposed surface functionalization, the engineered interface was used to assay tryptophan in real samples. Tryptophan (TRP) is an essential amino acid vital for human growth and is a precursor for numerous bioactive compounds, such as serotonin, melatonin, tryptamine, and nicotinamide[156,157]. Tryptophan has been associated with many diseases due to its vital function as a precursor of essential metabolites. Low levels of tryptophan in the body have been linked with various metabolic and neurological disorders, including depression, anxiety, insomnia, and mood swings[148,156,158]. Furthermore, the easy availability of over-the-counter supplements has endangered masses to higher doses of TRP, which has potentially adverse consequences. Therefore, it is critical to have a protocol for estimating tryptophan in human body fluids and food samples.

3.2 Result and Discussion

This chapter intends to report the synthesis, characterization, and application of BCN for improving the electrochemical performance of screen-printed electrodes (SPE) using an unconventional surface engineering approach. Thus, the following sections are adequately devoted to addressing the physicochemical features of the BCN, followed by its effective usage in the electro-functionalization of SPE.

3.2.1 Chemical and Physical Characterization of Boron Carbon Nitride

Boron carbon nitride was synthesized via the solvothermal process with boric acid and melamine as the B, C, and N sources, respectively. Various scientific tools were then

employed to confirm the effective synthesis of BCN as the end product. **Figure 3.1a** presents the X-ray diffraction patterns for the gCN, hBN, and synthesized BCN. The intense peaks in the recorded diffractogram clearly indicate the high crystallinity of the prepared material. Evidently, the material showcases a distinct and sharp peak at $2\theta = 27.97^{o}$, which corresponds to the (002) plane of BCN[159]. The peak is in agreement with the previously reported literature[160] confirming the formation of BCN. Nevertheless, the presence of melamine diborate[161] was also indicated from the XRD patterns. As illustrated in **Figure 3.1a**, the two possible binary phase materials of B, C, and N, namely hBN and gCN, exhibit strong peaks corresponding to the (002) plane at 26.67^{o} and 27.39^{o} respectively, suggesting the presence of similar honeycomb structure in all three materials[162,163]. The shift in the major diffraction peak towards a higher 2θ value manifests the decrease in the interlayer spacing of the layered structure from 3.34 Å in hBN to 3.25 Å in BCN. The decrease in interlayer spacing or lattice parameters can be explained by C having smaller atomic radii (70 pm) than B (85 pm)[164], resulting in shorter estimated bond lengths of C-N compared to B-N.

Vibrational spectroscopy was then employed to characterize the surface functionalities of the synthesized material. **Figure 3.1b** presents the FTIR spectrum of the synthesized BCN. Two distinct peaks were observed at 3390 and 3230 cm^{-1}, indicating the presence of O-H and N-H bonds, respectively[165,166]. The N-H bonds manifest the presence of free amine moieties on the terminals of unpolymerized borazine and triazine structures. On the other hand, the O-H bonds can be ascribed to the presence of moisture and oxide contaminants. The peak at 1196 cm^{-1} can be assigned to the B-O bond arising from melamine diborate, an intermediate compound in melamine and boric acid reaction[167]. A cluster of peaks in the range of 1400-1750 cm^{-1} indicates the presence of triazine and borazine rings in the synthesized material, which is also suggested by the presence of a characteristic peak at

806 and 766 cm^{-1}, respectively[167,168]. The peaks at 766 cm^{-1} and 1534 cm^{-1} are the characteristic peaks of the borazine ring corresponding to B-N-B out-of-plane bending and B-N in-plane stretching vibration, respectively[165]. Furthermore, the distinct peaks observed at 1380 and 1084 cm^{-1} are attributed to the B–N stretching and the cubic B–C vibrations, respectively, confirming the simultaneous inclusion of boron, nitrogen, and carbon in the ring. Thus, from the XRD and FTIR analysis, it was concluded that the synthesized material is BCN, which consists of triazine and borazine units cross-linked by hydrogen bonds[161].

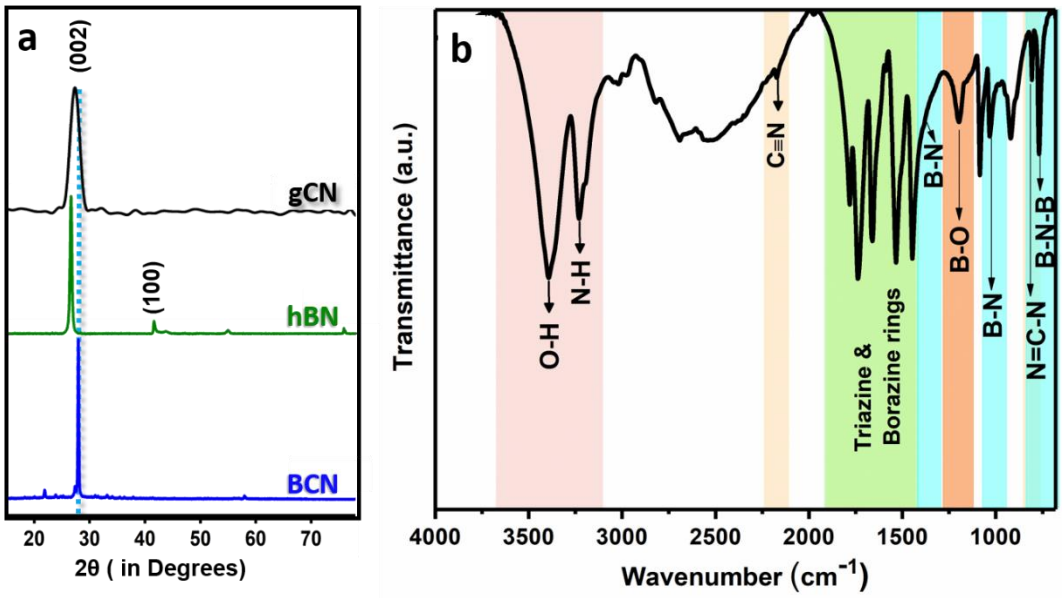

Figure 3.1 a) XRD patterns of hBN, gCN, and synthesized BCN material, **b)** FTIR spectra of synthesized BCN material.

HR-SEM images of BCN are shown in **Figure 3.2a**. The image depicts two-dimensional layered structures stacked on top of one another. The BCN layers were found to have severely etched edges, which can be clearly seen in **Figure 3.2b** and **Figure 3.2c**. The etching effect is expected to increase the surface area of the material, which will result in facile charge transfer. The probe sonication will upsurge the etching impact, leading to a

better suspension for electrochemical applications. Therefore, an SEM image of the BCN was also recorded after probe sonication, as shown in **Figure 3.2d**.

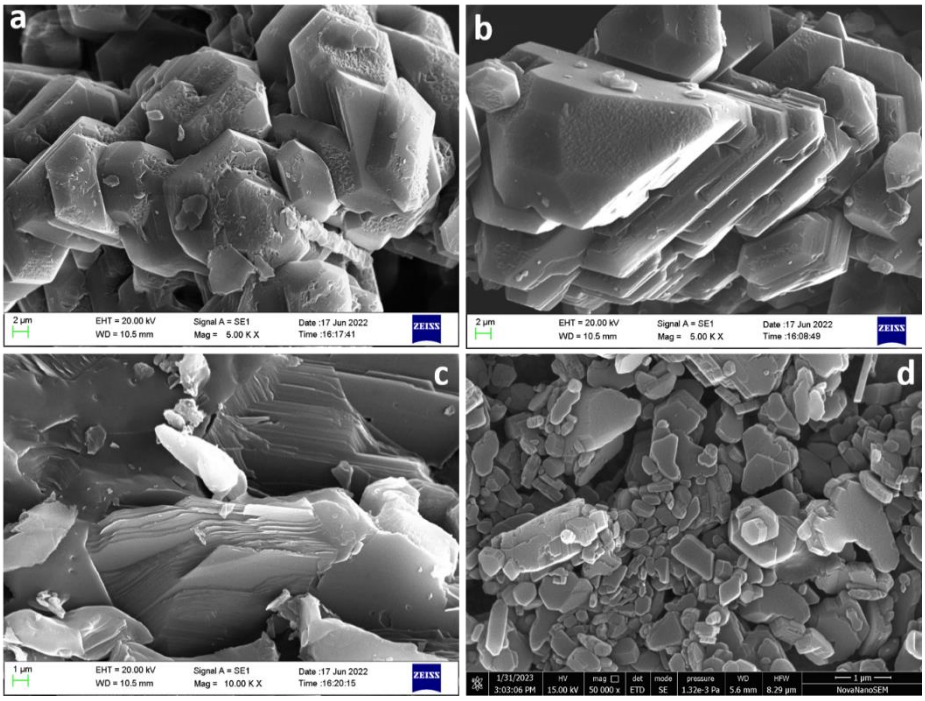

Figure 3.2: SEM images for the BCN material at different scales, **a)** 2 µm, **b)** 2 µm, and **c)** 1 µm, respectively, **d)** SEM image of BCN suspension prepared via probe sonication.

By comparing after and before sonication images, it can be univocally inferred that probe sonication resulted in significantly reduced particle size, leading to an increased surface-to-volume ratio, which is expected to be conducive to improving the electrochemical behavior of BCN. The compositional information of the material was derived by employing energy-dispersive X-ray spectroscopy (EDS) in conjunction with the HRSEM. The elemental mapping (**Figure 3.3**) verifies the simultaneous presence of boron, nitrogen, and carbon in the targeted area of material, thereby validating the successful synthesis of 2D BCN material. Consequently, the BCN suspension so obtained was next used for the electro-functionalization of SPE.

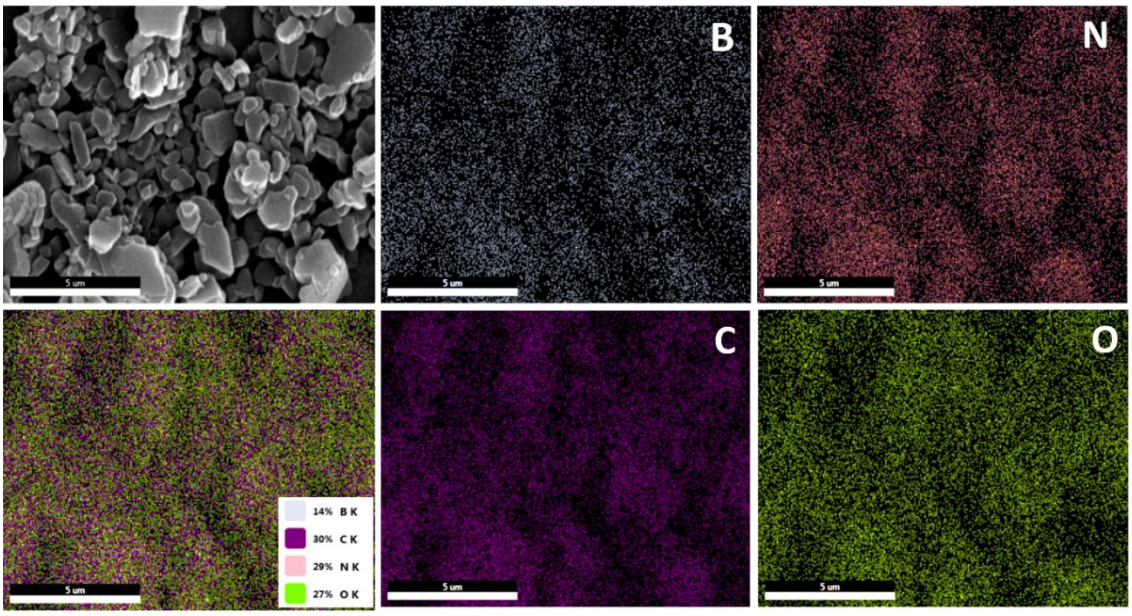

Figure 3.3 SEM image of the probe sonicated BCN material and the corresponding elemental mapping illustrating the presence of boron, carbon, nitrogen, and oxygen on the surface of BCN.

3.2.2 Electro-Functionalization Protocol: Optimization and Characterization

The screen-printed electrode surface was electrochemically functionalized with the BCN nanomaterial using cyclic voltammetry (CV) following the protocols discussed in the experimental section. The cyclic voltammograms corresponding to the electro-functionalization are presented in **Figure 3.4**a. In the first cycle, a distinct peak (peak I) is witnessed at 1.3 V, ascribed to the formation of radical cations from the oxidation of amine groups present in the BCN material[165,166]. These newly formed radical cations form dimers in the second cycle due to NH-NH coupling, which resulted in a reversible redox peak couple at 0.7 V (peak II) and 0.67 V (peak III), indicating the electro-polymerization of the BCN on the conducting surface. The peak IV at ~ 0.3 V corresponds to the monomer units. With the subsequent cycles, the current of peak III witnessed a gradual increase, indicating the growth of the BCN electrodeposited layer on the SPE surface as a result of the opted surface functionalization method.

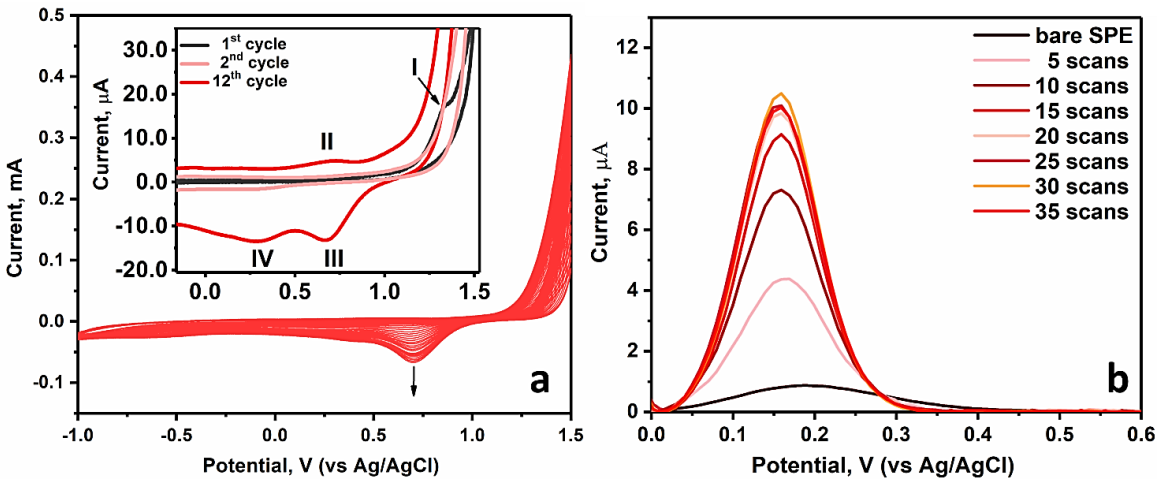

Figure 3.4 **a)** Cyclic voltammograms for electro-functionalization of BCN on SPE performed in the potential range -1 V - 1.5 V for 30 cycles; [Inset: 1st, 2nd, and 12th cycle magnified to point major peaks.] **b)** Differential pulse voltammograms recorded for varying number of cycles in 0.5mM $K_3[Fe(CN)_6]$ solution.

The thickness of the electrodeposited BCN material was next tuned to offer superior electrochemical performance by changing the number of CV scans from 5-35. The effect of the number of CV scans on the electrochemical performance of the SPE was probed by monitoring the respective current response in the $K_3[Fe(CN)_6]$ solution. As shown in **Figure 3.4b**, BCN functionalized SPE exhibited significantly enhanced peak current with a much-improved peak shape compared to the bare SPE. This indicates facilitated charge transfer at the BCN functionalized surface. Furthermore, the current was found to increase with the increasing number of cycles up to 30 scans, after which a slight depreciation in the current value was observed. Based on the results, 30 CV scans were chosen as the optimal number of scans for BCN-assisted electro-functionalization of SPE and used throughout the electrochemical studies.

Though the enhanced current responses clearly showcase the successful electro-functionalization of SPE with the BCN, the compositional characterization and

topographical changes of the modified surface were further investigated using X-ray photoelectron spectroscopy (XPS) and scanning electron microscope (SEM).

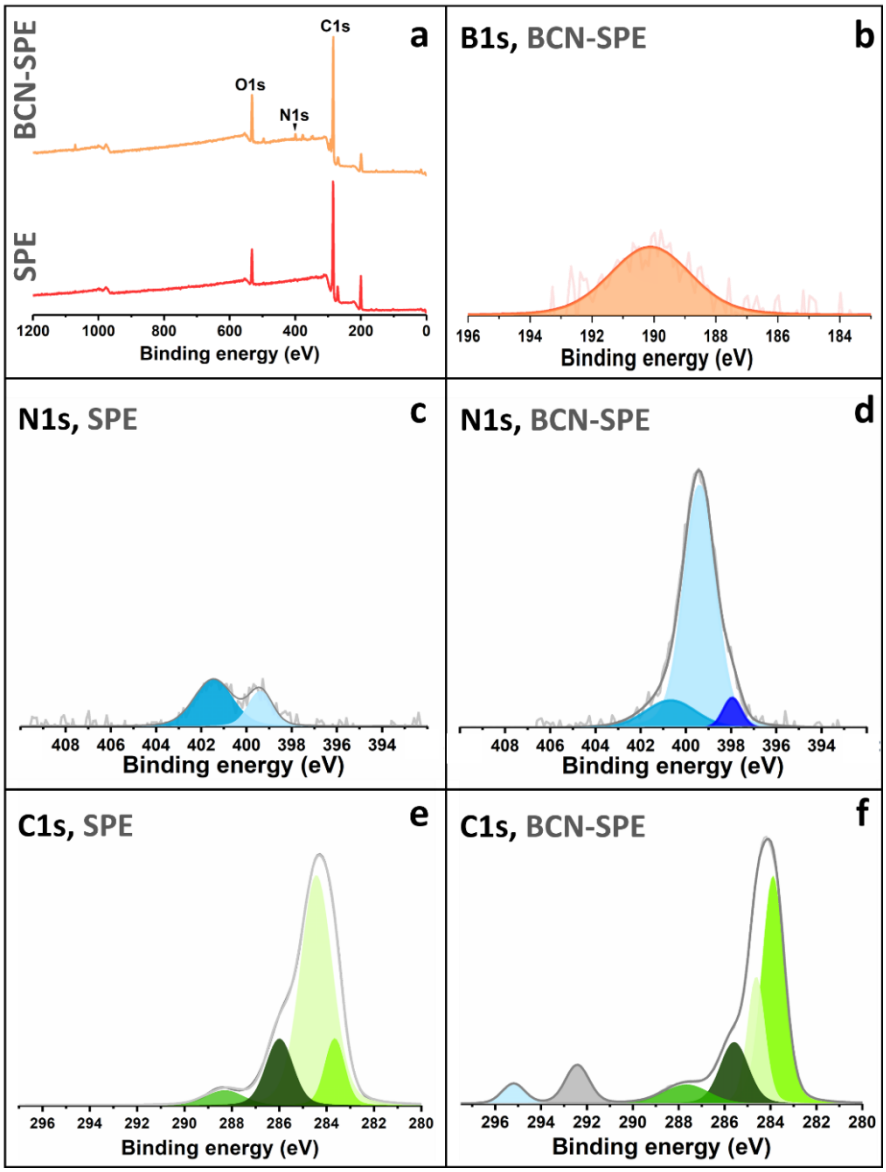

Figure 3.5 a) Full XPS survey of bare and modified SPEs **b)** deconvoluted core spectra of B1s of BCN-SPE, deconvoluted core spectra of N1s of **c)** bare SPE and **d)** BCN-SPE, deconvoluted core spectra of C1s of **e)** bare SPE and **f)** BCN-SPE.

Figure 3.5 depicts the full XPS Spectra recorded over the working electrode surface of the bare, and BCN-modified SPE, as well as the corresponding high-resolution spectrum for B, C, and N elements. While bare SPE was devoid of any contribution from boron, B1s

spectra of BCN-SPE showcase a peak at 190.5 eV, attributed to the B-N bonding resulting from the BCN electro-functionalization[167](**Figure 3.5b**). Similar conclusions were made from the N 1s high-resolution spectra (**Figure 3.5c and d**). The N1s spectra of bare SPE displayed two peaks corresponding to the surface C-N groups originating from the carbon ink used for manufacturing SPE. A sharp upsurge of the peak at 399.38 eV was observed in the case of BCN-SPE, indicating a significant increase in C-N functionalities compared to unmodified SPE[168]. Furthermore, the N1s spectra of BCN SPE showcase an additional peak at 397.88 eV, which can be ascribed to the presence of B-N bonds of the borazine rings[169]. The deconvoluted C1s spectra of bare SPE and BCN SPE show four peaks (**Figure 3.5e and f**) corresponding to the carbon-based working electrode of SPE. Specifically, the peak at 284.58 eV is attributed to the C=C bond, CH-CCl at 285.98 eV, C-N bond at 283.88 eV, Ag_2CO_3 at 288.48eV all arising from the graphite ink with added binders and organic solvents used for printing the SPE[170–172]. However, compared to unmodified SPE, a significant increase in C-N functionalities on the BCN-SPE is evident from the considerably enhanced peak intensity at 283.88 eV. The two additional peaks at 287.78 eV and 292.48 eV in the C1s spectra of BCN-SPE further confirm the presence of sp^2 hybridized C/C-N groups of the triazine rings which is one of the building blocks of boron carbon nitride. Therefore, XPS analysis demonstrates the effective electro-polymerization of BCN on the SPE.

A scanning electron microscope (SEM) was then used to examine the topographical changes caused by the BCN electro-functionalization. As presented in **Figure 3.6**, after modification, the ITO surface was found to be uniformly covered with evenly distributed nanostructures of BCN with relatively similar sizes. The figure not only provides visual evidence for the electro-polymerization of BCN on the conducting surface but also manifests the uniqueness of the electrodeposition strategy for in-situ exfoliation and

uniform surface decoration compared to conventional drop casting, which results in agglomerated structures. The nano-sized morphology of BCN on the modified surface is expected to increase surface area. While the data presented above confirms the successful functionalization of SPE with BCN and hints towards a consequent increase in its surface area, it is critical to determine whether this translates to an increase in the electroactive surface area of the electrode and hence was calculated in the following section.

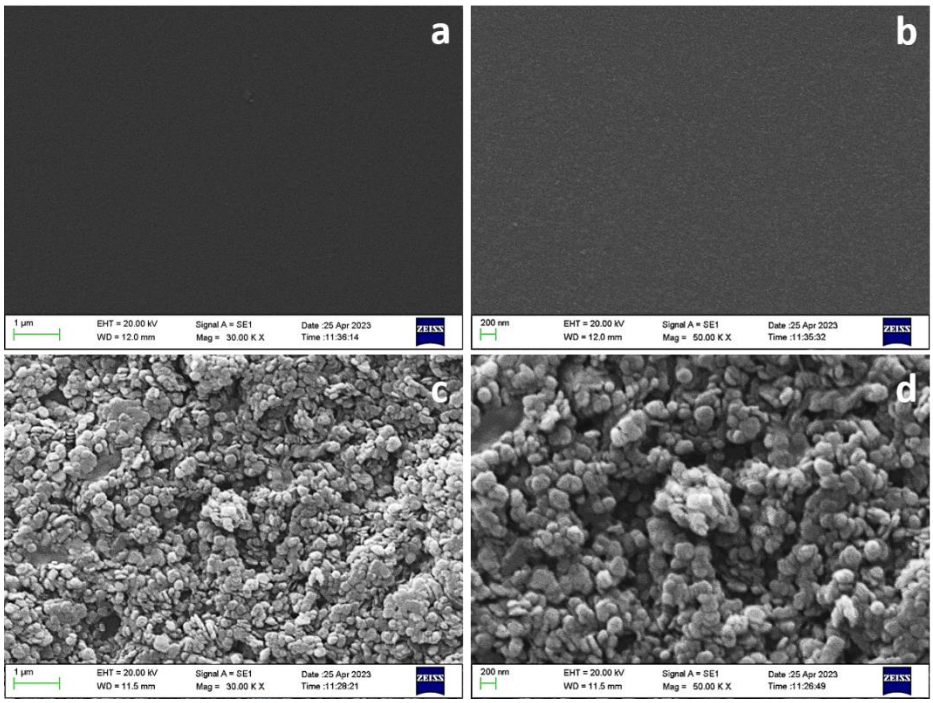

Figure 3.6 SEM images at 1 µm and 200 nm resolution of bare ITO **(a, b)** and BCN modified ITO **(c, d).**

For calculating the electroactive surface area of the bare and the modified SPE, the cyclic voltammograms for both SPEs were recorded at various scan rates ranging from 10-100 mV/s in an equimolar solution of 1 mM $K_3[Fe(CN)_6]$ and 1 M KCl. The voltammograms recorded using BCN-SPE show an oxidation peak at 219 mV and a reduction peak at 132 mV, with a peak separation of 87 mV, representing the redox couple with quasi-reversible attributes. No discernible potential shift was observed with the increasing scan rate. By employing the Randle-Sevcik equation,

$$\mathbf{I_p = \pm 2.69*10^5 n^{2/3} AD^{1/2} Cv^{1/2}}$$

where I_p represents the peak anodic/cathodic current (μA), A represents the electro-active area (cm^2), C represents the concentration of probe molecule (0.5 mM), n represents the number of transferred electrons, υ represents the scan rate ($V\ s^{-1}$) and D represents the diffusion coefficient ($D = 3.09 \times 10^{-6}\ cm^2\ s^{-1}$ for $[Fe(CN)_6]^{3-}$ in KCl solution), the electroactive area for the bare SPE came out to be 0.0139 cm^2. The calculated electroactive surface for BCN-modified SPE was found to be 0.0638 cm^2, which is ~ 5 times larger than the bare SPE. As expected, owing to the unique stoichiometry, SPE modification with BCN provides considerably more active sites for electron exchange. Error! Reference source not found. shows the comparative CV and DPV plots between the bare SPE and BCN-modified SPE in 0.5 mM $K_3[Fe(CN)_6]$ solution. As illustrated in Error! Reference source not found.**a**, the functionalization significantly lowers the over-potential needed for the oxidation and reduction of $K_3[Fe(CN)_6]$ redox couple while simultaneously enhancing the current response. The comparison of bare and modified SPE's DPV plots in Error! Reference source not found.**b** demonstrates the magnification of current response in the order of ~ 5 times, which conclusively proves the effectiveness of electro-functionalization with BCN in enhancing the electrochemical activity of SPEs. Following these outstanding results, the designed interface is investigated for sensing tryptophan, an essential amino acid for human beings.

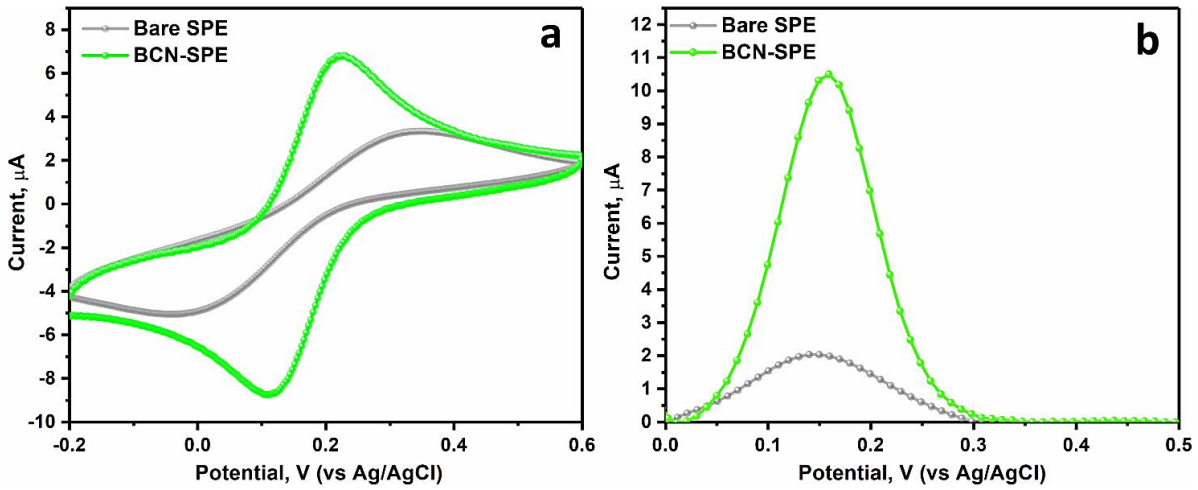

Figure 3.7 a) CV and b) DPV plots of bare and BCN-modified SPEs recorded in an equimolar solution of 1 mM $K_3[Fe(CN)_6]$ and 1 M KCl.

The electrochemical reaction kinetics of the modified electrode was investigated using electrochemical impedance spectroscopy (EIS). **Figure 3.8** illustrates the EIS spectra for bare, and BCN-modified SPEs recorded in 0.5 mM $[Fe(CN)6]^{3-/4-}$ a solution containing 1M KCl in the frequency range of 0.1 - 10^6 Hz. In the high-frequency range, a semicircle is observed corresponding to the charge transfer process, and the diameter reflects the charge transfer resistance (R_{ct}), whereas the low-frequency range corresponds to the diffusion process[173]. The fitted equivalent circuit suggests that the R_{ct} value for the bare electrode is 45.6 kΩ, which decreases significantly to 14.6 kΩ after modification with BCN. The increase in the low-frequency region and more inclination towards the imaginary axis further indicates improved diffusion kinetics, thereby easing the faradaic processes. The remarkable depreciation in the resistance can be attributed to the enhanced functionalities on the SPE surface, providing better pathways for charge transfer. The results are in good agreement with the CV and DPV plots, justifying the current amplification on BCN-modified SPEs.

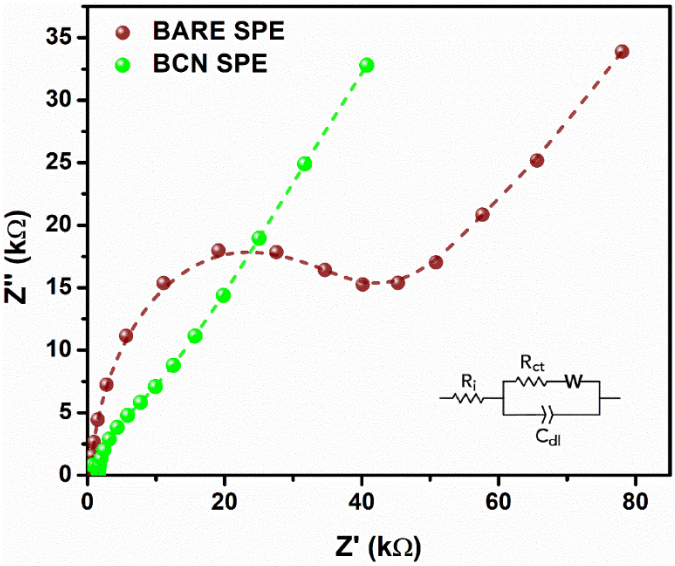

Figure 3.8 Electrochemical Impedance spectra for bare and BCN modified SPE and the equivalent circuit.

3.2.3 Applicability of the BCN- SPE Interface for Tryptophan Sensing

Experiments were conducted to investigate the influence of phosphate buffer pH on the behavior of the sensor towards tryptophan oxidation and to determine the optimum pH for further study. For this purpose, solutions containing 100 µM of TRP were prepared using phosphate buffer with different pH values. It was witnessed that the peak potential shifted towards lower values with increasing pH, indicating facilitated oxidation with higher pH (**Figure 3.9a**). The relationship between peak potential and pH is expressed in the following linear equation:

$$E_p\,(V) = -\,0.0468\ pH + 0.7518$$

The slope value was nearly -0.047, which is very close to the theoretical value of -0.059 corresponding to the oxidation behavior involving an equal number of electrons and protons[148]. Thus, it can be fairly assumed that the reaction involved two electrons and two protons, as illustrated in **scheme 1**.

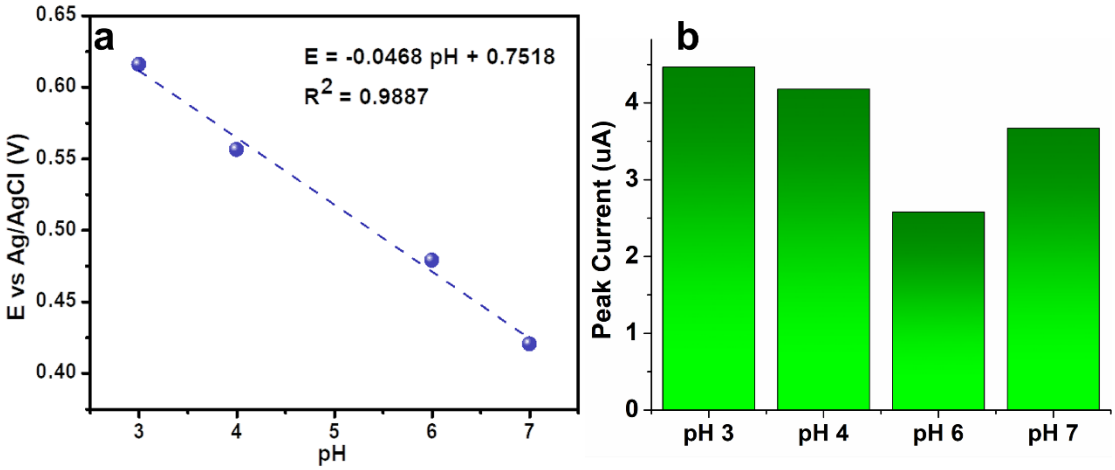

Figure 3.9 a) pH versus peak potential, and **b)** bar diagram depicting pH versus peak current recorded in 100 µM TRP.

Figure 3.9b shows the bar diagram of TRP peak current with different pH values. The observed results indicated that the solution with pH 3 exhibited the highest current, closely followed by solutions with pH 4 and pH 7. Despite the maximum response at pH 3, we opted to utilize pH 7 buffer solutions for our subsequent studies due to two primary reasons. Firstly, there was a significant peak potential shift towards lower values at higher pH solutions. Secondly, our objective involved the analysis of TRP concentrations in biological samples such as urine, blood serum, or food samples, which have pH values close to 7. Therefore, considering these factors, pH 7 was selected as the appropriate pH for the subsequent studies.

Scheme 1

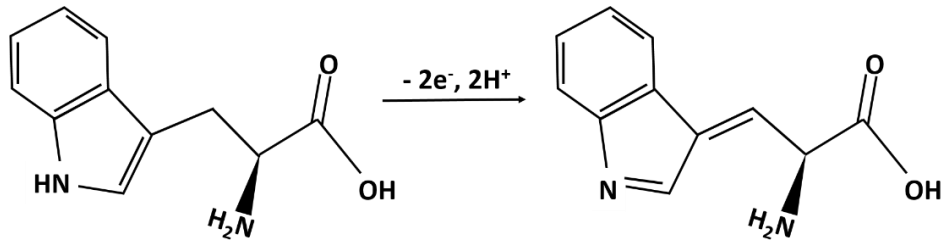

After optimization and in-depth characterization of the BCN electro-functionalized SPE, the modified electrode was employed for qualitative and quantitative analysis of tryptophan to test its real-world potential. **Figure 3.10a** shows the CV voltammograms recorded for 100 µM TRP using bare as well as BCN-modified SPE. As illustrated, TRP oxidizes at a peak potential of 0.52 V at BCN-SPE with a significant negative shift of 0.13 V compared to unmodified SPE. The shift of ~ 0.13 V indicates the electro-catalytic behavior of the modification specifically for the TRP, as no such shift was witnessed in the case of $K_3[Fe(CN)_6]$. Also, the DPV plot showcases that electro-functionalization with BCN has led to a nearly 5-fold increase in the current response of SPE, along with a shift of ~ 0.18 V (**Figure 3.10b**). This significant surge in current and negative shifts in the potentials can be attributed to the specific π- π interaction between the BCN and the aromatic ring of the tryptophan molecule, along with H-bonding and the enhanced electroactive area of the electrode. These interactions bring the TRP molecule closer to the interface, facilitating charge transfer and resulting in oxidation at lower potentials. To conduct a more rigorous quantitative inspection, the calibration curve was plotted by monitoring the impact of varying TRP concentrations on the corresponding current responses using both bare and BCN-SPE.

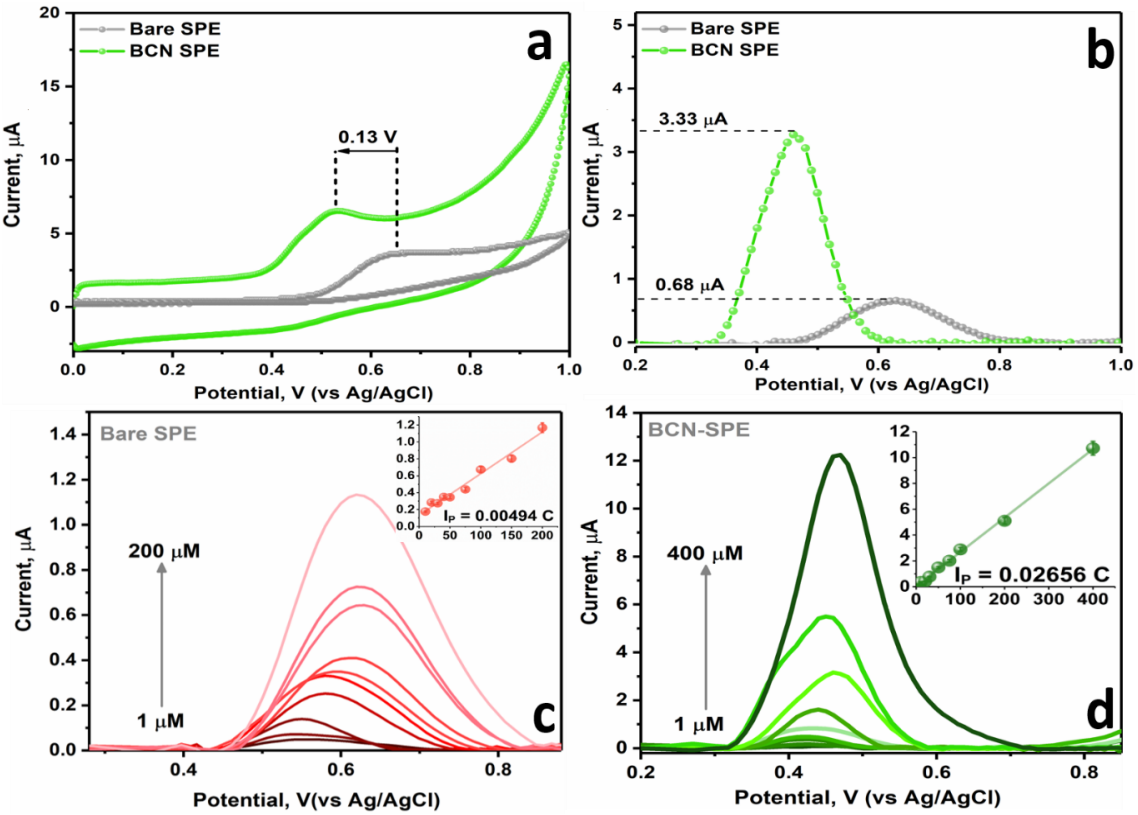

Figure 3.10 a) Cyclic voltammograms and **b)** differential pulse voltammograms recorded in 100µM tryptophan solution at bare and BCN-modified SPE. **c)** Differential pulse voltammograms were recorded on bare SPE for concentrations 1 µM,5 µM,10 µM, 20 µM, 30 µM, 40 µM, 50 µM, 75 µM, 100 µM, 150 µM, and 200 µM; [**inset:** Calibration plot shown for TRP concentrations from 10-200 µM]. **d)** Differential pulse voltammograms were recorded on modified BCN-SPE for concentrations 1 µM, 5 µM, 10 µM, 20 µM, 30 µM, 50 µM, 75 µM, 100 µM, 200 µM, 400 µM; [**inset:** Calibration plot shown for TRP concentrations from 1-400 µM].

For conducting the concentration study, the current responses were recorded using the DPV in the concentration range of 1-400 µM using bare and BCN-modified SPE. As depicted in **Figure 3.10c**, TRP oxidation occurs at ~ 0.60 V potential at the surface of bare SPE. The peak current was found to increase with the increasing TRP concentration in the range of 10-200 µM. Below 10 µM, no differentiable current response for TRP oxidation

was observed using bare SPE. Notably, a considerable shift in the peak potential can be witnessed with the increasing concentration, which is attributed to the complex electro-oxidation mechanism involving the formation and adsorption of intermediate products[174]. The BCN-SPE exhibited a current response for much lower levels of TRP concentrations (1 µM), which is a manifestation of significantly enhanced sensitivity of the surface. **Figure 3.10d** depicts the linear increase in the peak current with increasing TRP concentrations. The improved peak shapes and enormously magnified current response attest to the facilitated charge transfer at the BCN electro-functionalized surface. The relation between concentration and its corresponding oxidation peak current of the two surfaces is presented in the two linear regression equations,

$Y = 0.00494[10\mu M - 200\mu M] + 0.13176$, $R^2 = 0.97825$ (Bare SPE)

$Y = 0.02656[1\mu M - 400\mu M] + 0.0471$, $R^2 = 0.9989$ (BCN - SPE)

From the above linear equations, it was concluded that the engineered BCN SPE exhibited approximately a five-fold increase in sensitivity compared to the bare electrode. The limit of detection (LOD) for bare and modified SPE was also calculated using the following formula

$LOD = 3S/b$,

Where S stands for a standard deviation of blank measurements, and b is the slope of the calibration plot.

The LOD for BCN-SPE was calculated to be 36.4 nM, which is reasonably lower than the 209 nM for bare SPE. This significant drop in the limit of detection (LOD) for tryptophan is due to a combination of two factors: increased surface area and the specific π-π interaction between BCN and tryptophan aromatic ring, which facilitated the charge transfer, thereby increasing the responsiveness of the sensing platform. In addition, the modified sensor showcased an exceptional sensitivity of 0.42 $\mu A \mu M^{-1} cm^{-2}$, underscoring

its remarkable ability to detect minute concentrations of TRP. Furthermore, when compared to other recently reported electrodes (**Table 3.1**), our sensor demonstrated significantly lower detection limits for TRP.

Next, we performed the scan rate study to rule out any possible adsorption complications arising from the surface functionalization. Cyclic voltammograms of the BCN-modified SPE were recorded in 100 µM TRP solution at different scan rates ranging between 25 - 500 mV/s (**Figure 3.11a**). **Figure 3.11b** and **Figure 3.11c** shows the plots of oxidation peak currents as a function of scan rate (ν) and the square root of scan rate ($\nu^{1/2}$), with the corresponding linear regressions recorded in the equations below.

I_p (µA) = 0.0504 ν [25 – 500 mV/s] + 0.6754; R^2 = 0.9749

I_p (µA) = 0.4227 $\nu^{1/2}$ [25 – 500 mV/s] + 0.1356; R^2 = 0.9927

Since the peak current demonstrates excellent linear correlation with the $\nu^{1/2}$, it can be inferred that the reaction at the interface is diffusion-controlled, and the enhanced electroactive area of the electrode doesn't add any adsorption complications during the electrochemical process[175].

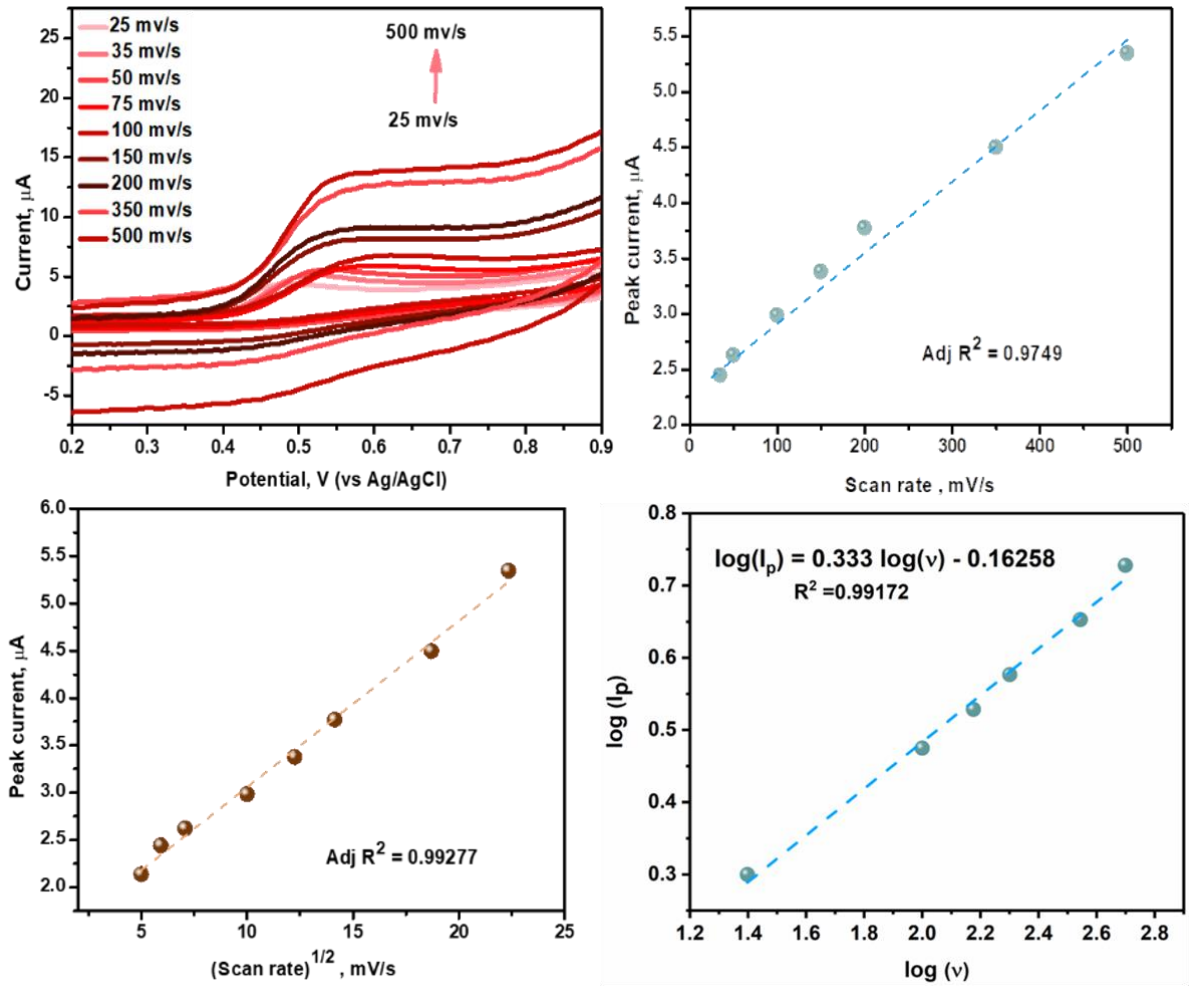

Figure 3.11 a) Cyclic voltammograms were recorded for a fixed concentration of TRP (100 µM) at different scan rates of 25 mV/s, 35 mV/s, 50 mV/s, 75 mV/s, 100 mV/s, 150 mV/s,200 mV/s, 350 mV/s, 500 mV/s. Plots corresponding to **b)** peak current versus scan rate. **c)** peak current versus (scan rate)$^{1/2}$. **d)** log (peak current) versus log (scan rate).

Furthermore, the plot between the logarithm of peak current and the logarithm of scan rate follows a straight line as depicted in **Figure 3.11d** with a slope of 0.33, which is close to the theoretical value of 0.5, again confirming that the electrode process is primarily diffusion controlled[148].

Table 3.1 Comparison of BCN modified sensor with recently reported modified surfaces for the measurement of TRP.

Working electrode	Linear range (µM)	LOD (µM)	Drawbacks	Reference
Cs/Ce-MOF	0.25-331	0.14	Toxic and expensive metal-based systems, complicated synthesis	[176]
Nafion/TiO_2-graphene/GCE	5-140	0.7	Multi-component system	[177]
$CeVO_4$ /GCE	0.1-94	0.024	Toxic and expensive metal-based systems	[178]
Au NPs /GCE	0.85-1200	0.08	Expensive, Drop cast based	[179]
Graphite	5-150	1.73	Large Electrodes	[174]
AHNSA /rGO/GCE	0.05-200	0.031	Multi-component system	[180]
QDs/GA/PPD/SPCE	100-500	14.7	Multi-component system, High LOD	[181]
BCN-SPE	1-400	0.036	Single component, facile and optimized protocol, portable, cost-effective	This work

The above results showcase the unique ability of the modified SPE surface to assess the concentration of tryptophan qualitatively and quantitatively in a test sample. However, in body fluids and food samples, tryptophan co-exists along with numerous other

biomolecules. The presence of these biomolecules can potentially alter the responses of our sensor, leading it to furnish incorrect results. Therefore, there is a requirement for conducting sensing experiments in complex matrices to assess the selectivity of the sensor.

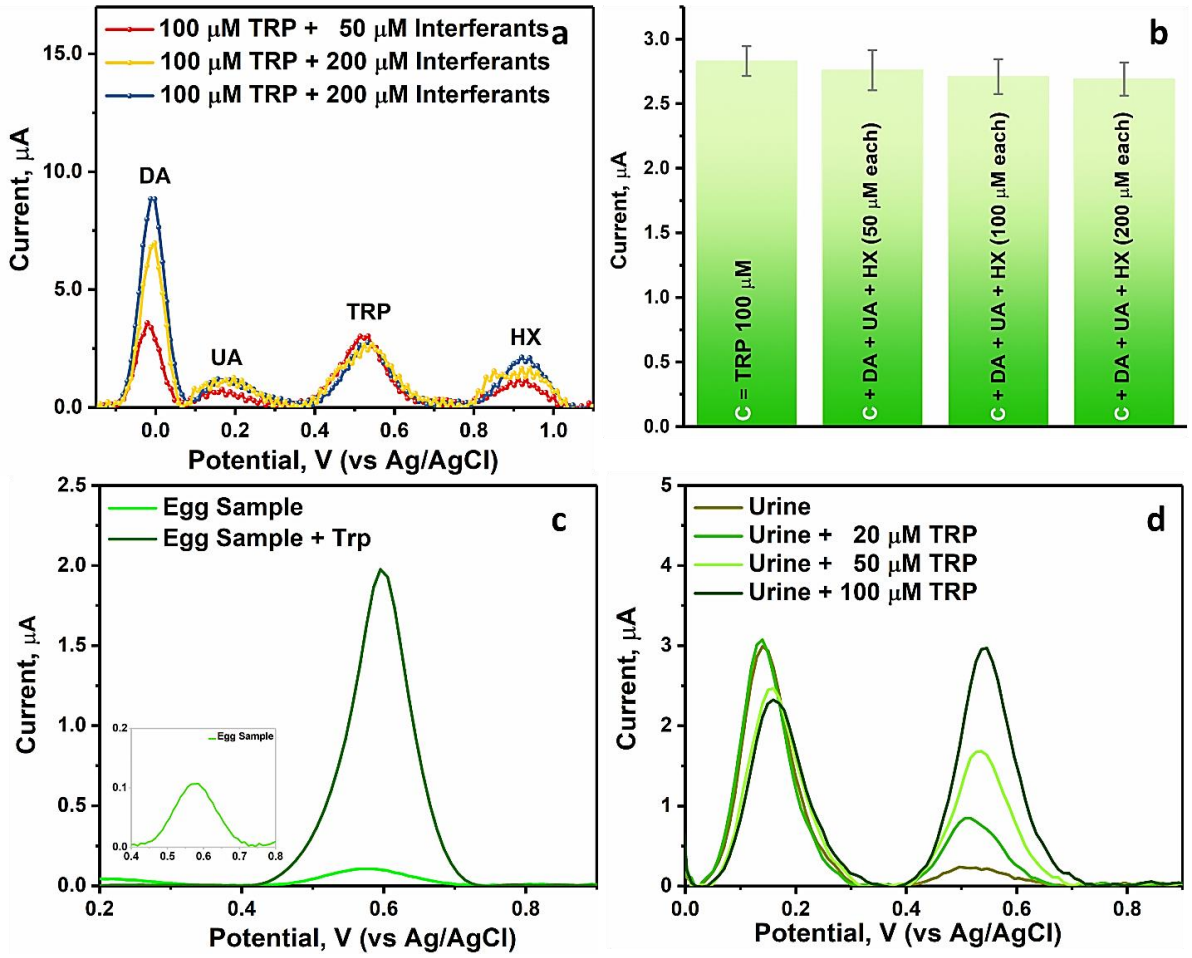

Figure 3.12 a) Differential Pulse Voltammograms recorded for a fixed concentration of TRP (100 µM) with increasing concentrations of interference at 50 µM, 100 µM, 200 µM, and 500 µM. **b)** Graph depicting the current responses at 0.55 V specific to tryptophan in the presence of varying concentrations of dopamine (DA), uric acid (UA), and hypoxanthine (HX) (95% confidence interval). Differential Pulse Voltammograms were observed for **c)** Egg white solution and **d)** human urine sample.

2.1.1.6 Interference studies

Solutions containing varying amounts of commonly found biomolecules such as dopamine, uric acid, hypoxanthine, and tryptophan were subjected to differential pulse potential, and their corresponding current responses were recorded, as illustrated in **Figure 3.12a**. The concentration of tryptophan was kept constant (100 µM) in all the solutions. Evidently, the peaks of DA, UA, and HX showed enhanced current response with increasing concentration, but the peak corresponding to tryptophan demonstrated constant current and potential without any significant deviation. The results indicate that the sensor exhibits satisfactory selectivity and holds the potential for practical application in sensing real samples. Compared with the current response of 100 µM tryptophan in the test sample, the solutions containing interferents showed a minimal deviation of <5%, as represented through a bar diagram in **Figure 3.12b**.

2.1.1.7 Real sample study

Following the success of the interference study in the test matrix, the sensor performance was evaluated in two real samples, namely egg white and human urine. The choice of a food sample and a human body fluid was made to demonstrate the developed sensor's applicability in the healthcare and food industries. Egg white, a rich source of protein and amino acids, including tryptophan, was selected as a food source. Whereas the loss of TRP in urine is considered a biomarker for several diseases associated with the excessive breakdown of proteins and reduced intestinal absorption. As a result, the developed sensor's ability to quantitatively estimate TRP in urine was tested using human urine as the second sample.

2.1.1.8 Egg sample

The presence of TRP was estimated in the egg white sample by recording a DPV response in the diluted egg white solution. As shown in **Figure 3.12c**, the DPV showcased a peak at 0.55 V, which was found to increase with the TRP spiking, confirming that the peak was caused by TRP oxidation present in the egg white. The observed peak current was translated to the concentration of tryptophan using the calibration plot. The actual concentration of the tryptophan was estimated by utilizing UV-visible spectroscopy. The results are tabulated in **Table 3.2**, showcasing a good agreement between the TRP concentrations quantified using the developed sensor and the ones observed using UV-Vis spectroscopy with an error of ~ 3.93 %.

Table 3.2 Determination of tryptophan concentration in egg white sample by BCN-SPE and its validation using UV-vis spectroscopy.

Observed concentration (UV-Vis)	Observed concentration (sensor)	Error (%)
2.29 µM	2.38 µM	3.93

2.1.1.9 Urine sample

The DPV was next recorded in the diluted urine sample of a healthy volunteer. Interestingly, DPV showcases two peaks at 0.33 V and 0.59 V (**Figure 3.12d)**, corresponding to uric acid and TRP oxidation, respectively. The peak at 0.59 V increased with increasing concentrations of spiked TRP levels, confirming that the peak was caused by the oxidation of TRP in the urine sample. The TRP concentration in the diluted and spiked urine samples was calculated using the peak currents. UV-Vis spectroscopy was used to validate the results obtained using the developed sensor. The observed results are documented in **Table 3.3**. The observation manifests the presence of ~ 7.9 µM TRP in five

times diluted urine sample[182]. The results obtained using the developed sensor are in accordance with the concentrations observed using UV-vis spectroscopy, demonstrating an error of < 4.5 %. After analyzing both the real samples, it can be confidently said that the developed sensor can accurately monitor TRP levels in the complex matrix, such as food and human body fluids.

Table 3.3 Determination of Tryptophan concentration in spiked urine samples and their validation using UV-vis spectroscopy.

Spiked TRP (μM)	**Observed concentration** (μM) (UV-vis)	**Observed concentration (**μM) (Developed Sensor)	**Error (%)**
0	7.952	7.989 ± 0.378	3.70
50	57.961	60.428 ± 2.650	4.25
100	107.948	105.768 ± 4.882	2.01

2.1.1.10 Electrode stability and reproducibility

For practical applications, it is crucial for the developed SPE to have a moderate shelf life. As a result, we aim to monitor the electrochemical responses over a span of 28 days. For this purpose, three SPEs were electro-functionalized with BCN, and their current response corresponding to 75 μM TRP in phosphate buffer (pH 7) was recorded on day 1, day 14, and day 28 from the day of modification. According to the bar diagram shown in **Figure 3.13a**, BCN-SPE showed good stability with 95% peak current retention after 28 days. Further, the reproducibility of modification was tested using five SPEs, modified simultaneously with BCN, and their current response was recorded in 0.5 mM $K_3[Fe(CN)_6]$ solution using DPV, as shown in **Figure 3.13b**. The obtained results exhibit good overlap in terms of current and peak potential, thereby confirming the reproducibility of the modification with a consistently repeatable current response.

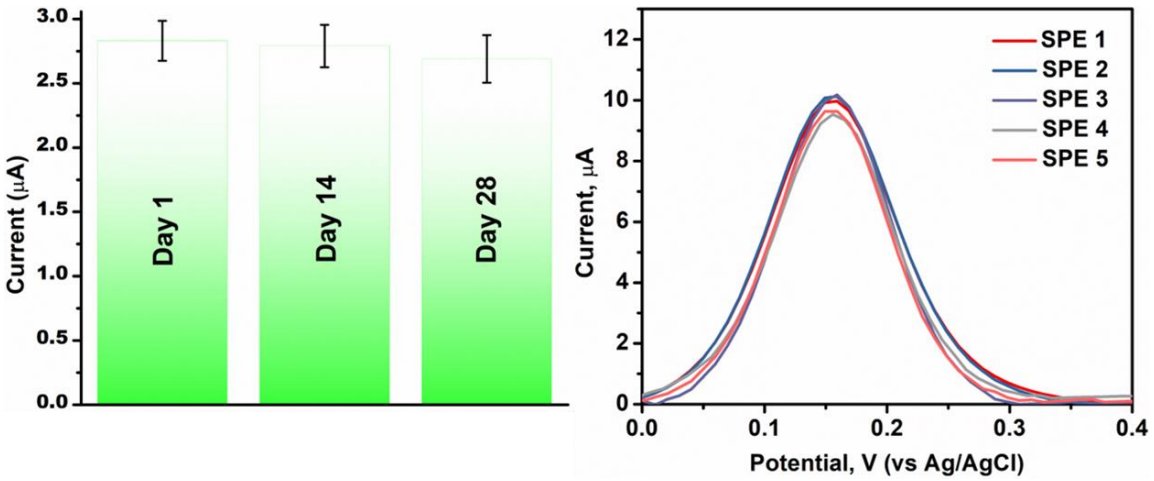

Figure 3.13 (a) Bar diagram of current response of BCN-SPE in TRP (75 µM) on day 1, day 14, and day 28. **(b)** Differential pulse voltammograms of five different BCN-SPE were recorded in 0.5 mM $K_3[Fe(CN)_6]$ solution to showcase the reproducibility.

3.3 Conclusion

This chapter uniquely reports the synthesis and electro-polymerization of boron carbon nitride on the screen-printed electrode. In this study, we report for the first time the mechanism underlying BCN electro-polymerization with an in-depth analysis of polymerization parameters on the electrochemical response of the screen-printed electrode. The chemical composition and the surface morphology of the modified SPE were inspected by employing XPS and SEM, respectively. The electro-polymerization resulted in a nearly fivefold increase in electroactive surface area with substantially higher surface functionalities offering effective interactions with the analyte. As a result, the BCN SPE manifested high sensitivity and selectivity for detecting tryptophan, an essential amino acid with a wide range of clinical implications, even in the presence of potential interfering molecules like uric acid, dopamine, xanthine, etc. The LOD calculated for the modified surface (36.4nM) was significantly lower than the bare SPE (209nM). Furthermore, the developed sensor was instrumental in detecting TRP in complex matrixes like human urine and egg whites. Our proposed method offers a low-cost, user-friendly, and portable alternative to traditional techniques for tryptophan detection, such as LC-mass

spectrometry and optical techniques which are very instrument-extensive and needs arduous pre and post-sample processing, making it an ideal candidate for point-of-care testing. This novel approach for electrode modification using electro-functionalization holds promise for developing advanced sensors for detecting various analytes in real-world settings, which could transform the field of analytical chemistry.